Pis'ma v ZhETF, vol. 85, iss. 5, pp. 288 – 293 © 2007 March 10

Strong space plasma magnetic barriers and Alfvénic collapse

E. A. Kuznetsov[+*], *S. P. Savin*[*], *E. Amata*[□], *M. Dunlop*[△], *Y. Khotyaintsev*[∇], *L. M. Zelenyi*[*], *E. V. Panov*[*◇], *J. Büchner*[◇], *S. A. Romanov*[*], *J. Blecki*[°], *J. L. Rauch*[⊥], *B. Nikutowski*[◇]

[+] *L.D. Landau Institute for Theoretical Physics RAS, 119334 Moscow, Russia*

[*] *Space Research Institute RAS, 117997 Moscow, Russia*

[□] *Istituto di Fisica dello Spazio Interplanetario, INAF, 00133 Roma, Italy*

[△] *Space Science and Technology Department, Rutherford Appleton Laboratory, OX110QX Chilton, UK*

[∇] *Swedish Institute of Space Physics, 75121 Uppsala, Sweden*

[◇] *Max-Planck-Institut für Sonnensystemforschung, 37191 Katlenburg-Lindau, Germany*

[°] *Space Research Center, Polish Academy of Sciences, Warsaw, 00716 Poland*

[⊥] *Laboratoire de Physique et Chimie, de l'Environnement, CNRS, Orléans, 45071 France*

Submitted 7 September 2006
Resubmitted 7 February 2007

We propose to interpret high-magnitude magnetic barriers in space and solar plasma as due to pile-up of magnetic field lines and their Alfvénic collapse for MHD flows. The analysis of experimental data of both Interball and Cluster spacecrafts shows that high-magnitude magnetic structures found in the Earth magnetosheath and near the magnetopause are supported by a nearly thermal transverse plasma flow, with the minimum barrier width being of the order of the ion gyroradius. The collapse termination at such scales can be explained by the balance between pile-up of magnetic field lines and backward finite-gyroradius diffusion. Intercomparison of the theory, modeling and experimental data points out that the Alfvénic collapse is in general a promising mechanism for magnetic field generation and plasma separation.

PACS: 52.30.−q, 52.40.Hf, 52.40.−w

1. Narrow high-magnitude magnetic barriers, which separate different flow regimes and display a magnetic pressure of the order of the plasma pressure, are often seen both in the space and solar plasma [1 – 3]. Haerendel [1] observed such structures in HEOS 2 data and attributed them to the work of streamlining magnetosheath flow over the magnetopause boundary layer. More recently such barriers have been usually regarded, near the Earth, as multiple magnetopause (MP) crossings or as a particular kind of flux transfer events. However, no particular mechanism has ever been accepted up to now to account for the anomalous rise of magnetic field magnitude $|\mathbf{B}|$. Some examples of such barriers were found in Interball-1 data and were described by [2]. It was argued that these barriers are neither MP nor shock crossings, have transverse scales down to the ion gyroradius, ρ_i, and separate flowing from stagnant plasma. In this Letter, for the first time we describe barrier events seen by Cluster and compare them with published, but so far unexplained, Interball barriers. We suggest Alfvénic collapse [4] as the generation mechanism for such barriers, study their growth and propose that their saturation be due to the ion finite-gyroradius effect. Moreover, we discuss a statistical set of magnetic barriers built upon 1995–2000 Interball-1 data. Finally, we argue that this mechanism can account for magnetic field filamentation and rise at the convection cell boundaries on the Sun [3].

2. The concept of Alfvénic collapse as a process of magnetic line pile-up (or breaking) in the framework of the ideal MHD approximation was introduced in paper [4]. Alfvénic collapse is due to plasma flowing obliquely to the magnetic field and leads, in 3D, to the local infinite increase of magnetic field intensity. This process is analogous to the breaking of vortex lines for fluids at high Reynolds numbers (see [5 – 7]) when the governing equations are the Euler equations.

The magnetic field $\mathbf{B}$ in ideal MHD obeys the induction equation,

$$\frac{\partial \mathbf{B}}{\partial \mathbf{t}} = \mathrm{curl}[\mathbf{v} \times \mathbf{B}], \tag{1}$$

which is analogous to the vorticity equation in Euler hydrodynamics. In a high β homogeneous plasma, the velocity field $\mathbf{v}$ can be considered as incompressible, i.e.

$\operatorname{div}\mathbf{v} = 0$. The same assumption can be made for very slow flows. Since only the velocity transverse to the local magnetic field, $\mathbf{v}_\perp$, is relevant in this equation, we introduce new Lagrangian trajectories

$$\mathbf{r} = \mathbf{r}(\mathbf{a}, t), \qquad (2)$$

defined in terms of $\mathbf{v}_\perp$

$$\frac{d\mathbf{r}}{dt} = \mathbf{v}_\perp(\mathbf{r}, t), \quad \mathbf{r}|_{t=0} = \mathbf{a}. \qquad (3)$$

Because the magnetic field is frozen in the plasma, equation (3) provides the equation of motion for magnetic field lines.

In terms of the mapping (2), equation (3) yields partial integration of Eq. (1) (for details see [4]):

$$\mathbf{B}(\mathbf{r}, t) = \frac{(\mathbf{B}_0(\mathbf{a}) \cdot \nabla_{\mathbf{a}})\mathbf{r}(\mathbf{a}, t)}{J},$$

where $\mathbf{B}_0(\mathbf{a})$ is the initial magnetic field, and J is the Jacobian of the mapping:

$$J = \frac{\partial(x_1 x_2 x_3)}{\partial(a_1 a_2 a_3)}.$$

It is evident that, as in common cases $\operatorname{div}\mathbf{v}_\perp \neq 0$, the mapping (2) will be compressible and there will be no restrictions on the Jacobian values. In particular, if the Jacobian vanishes, the magnetic field will reach infinity. In the general situation such type of events, called in [4] as breaking of magnetic lines, can occur at different locations in space. Physically this process is analogous to the appearance of shocks in gas-dynamics. Unlike breaking in gas-dynamics, in MHD this corresponds to a magnetic line touching another one, which yields an infinite magnetic field. Because in a high β plasma the slowest plasma flows are connected with Alfvénic excitations, the magnetic line pile-up can be called Alfvénic collapse. The main driving cause of the breaking is connected with the plasma flow *oblique* to the magnetic field direction. In this case the flow transverse to the magnetic field compresses bundles of magnetic lines swept by the flow. The occurrence of such events was found to be unlikely in two dimensions but possible in three dimensions [4].

The process of magnetic line pile-up can be considered also as a possible mechanism of magnetic field generation. Unlike classical dynamo, this process is of the blow-up type, so that, for ideal MHD, the magnetic field increases indefinetely.

However, the applicability of such a process to a real system has several limitations: 1) the magnetic Reynolds number must be large enough that the effects of finite conductivity can be neglected; 2) the compression of magnetic lines resulting in the increase of magnetic field intensity and of its gradients can continue only down to the ion gyroradius scale, where the MHD approximation and magnetic field frozenness break down. We suggest that the magnetic field pile-up at the barrier gradients can stop due to backward finite-gyroradius diffusion of the growing magnetic field. On these grounds, we can estimate the resulting equilibrium flow at the ion gyroradius scale from

$$\Delta(D_H\mathbf{B}) + \operatorname{curl}[\mathbf{u} \times \mathbf{B}] = 0, \text{ or } \mathbf{u}_\perp = D_H \frac{\mathbf{B} \times \operatorname{curl}\mathbf{B}}{|\mathbf{B}|^2}.$$

Here we assume that the diffusion coefficient for the magnetic field, D_H, can be estimated through a characteristic displacement of the order of the proton gyroradius, as Savin et al. [2] demonstrated that the gradient scale at the barrier edges and the barrier width tend to approach the proton gyroradius. Thus, $D_H = \rho_i^2/\tau$, where ρ_i is the thermal ion gyroradius and the characteristic diffusion time τ is taken to be of the order of the ion gyroperiod, as further argued in the discussion of Fig.1d. Recalling the spatial scale of the order of ρ_i, one gets the transverse (drift) velocity of the order of ion thermal velocity V_{Ti}:

$$u_\perp \sim V_{Ti}, \qquad (4)$$

that, as we will see below, matches fairly well both Interball and Cluster experimental data.

3. In Interball-1 data we found more than 200 strong barriers in the magnetospheric boundary regions with δB comparable or larger than the surrounding $|B|$ (see Fig.3 and related discussion herein). We were stimulated by these findings to further explore the possibility that Alfvénic collapse can be the cause of the barrier formation.

In the following, we make use of space borne data for two separate Cluster events, close to the MP, to infer an order-of-magnitude estimate of the Alfvénic collapse equilibrium state at ion-gyroradius scale gradients. We base our discussion on Cluster proton, electric and magnetic field data, but neglect magnetosheath (MSH) electrons, due to their smaller temperature and mass. Moreover, we base our discussion on the moments of the ion distribution function (density, velocity and temperature) having checked that they are practically isotropic around the analyzed magnetic barriers (see Fig.1 description further on).

On March 24, 2001, Cluster [8] first crossed the northern cusp MP on an outbound orbit at 09.00 UT when the spacecraft (SC) position was ($X = 10\,R_E$, $Y = 1\,R_E$, $Z = 15\,R_E$) in Geocentric Solar Ecliptic

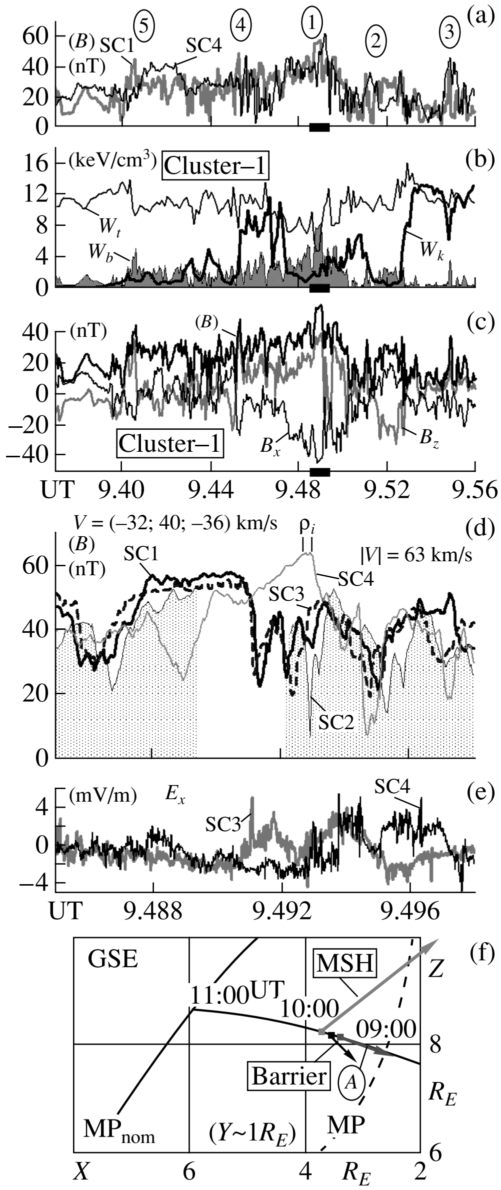

Fig.1. Cluster data on March 24, 2001. (a): $|B|$ for Cluster SC1 (thick line) and SC4 during an extended time interval of MSH BL crossing (the same interval is used for 1b-c); (b): SC1 proton ram pressure (W_k, thick line), proton thermal pressure (W_t), and magnetic pressure (W_b, shadowed line). (c): SC 1 GSE B_x, $|B|$ (thick line), and B_z (grey line). (d): close-up of the total magnetic field $|B|$ for SC1, SC2, SC3 and SC4 (thick, shadowed, dashed and thin lines respectively) around the main barrier, (e): close-up of GSE E_x for SC3 and SC4 (thick and thin lines) around the main barrier. (f): Cluster orbit (8–11 UT) projected onto the GSE XZ plane. Nominal MP ("MPnom", thick line), first MP encounter ("MP", dashed line), MSH, barrier and plasma velocities (marked "MSH", "Barrier" and "A" respectively)

(GSE) coordinates. The Cluster tetrahedron was such that the SC's were at about 600 km from each other and SC's 1 through 3 were forming a triangle roughly perpendicular to the average orbit (see Fig.1f), while SC4 was trailing the others. Figs.1a–1c display an overview of data measured by the 4 Cluster satellites in the MSH boundary layer from 9.37 to 9.56 UT. Fig.1a shows that $|B|$ from SC1 and SC4 exhibited several increases, among which we have highlighted the 5 most prominent ones (with amplitudes more than 2 times larger than background), which we call hereafter "barriers", marked with circled numbers. Barrier 1 is referred hereafter as the "main" barrier and its main peak is marked on each x axis by a black box.

Fig.1b displays SC1 ram, thermal and magnetic pressures defined as $W_k = N_i M_i V_i^2/2$, $W_t = N_i T_\perp + N_i T_{||}/2$, and $W_b = B^2/8\pi$, respectively (here, $T_{||}$ and $T_\perp$ are the parallel and perpendicular temperatures, N_i is the density and V_i is the mean ion velocity). First of all we observe that W_k increases from the quasi stagnant flow on the left (closer to the MP), where $W_t/W_k \gg 1$, to the normal MSH flow on the right, where $W_t/W_k \sim 1$. During most of the displayed period $W_t/W_k \gg 1$ and $W_t \gg W_b$, i.e. $\beta \gg 1$. Both such conditions justify the use of the high-β incompressible MHD approximation in equation (1). In particular, this is true at barriers 5, 4 and 2, which look similar to one another, and inside barrier 3 occurring after the ram pressure increase at 9.53 UT. Finally we notice that the decrease of W_t in barrier 1 described in Fig.1b is due mostly to a decrease of the perpendicular temperature $T_\perp$.

Fig.1c shows the SC1 magnetic field intensity, $|B|$, and its GSE components B_x and B_z We notice that at all barriers B_z displays a large positive increase. This rules out the possibility that at such times the spacecraft underwent a double crossing of the MP, as in that case a negative B_z should have been sampled. At all barriers each component generally displays a variation of the order of the $|B|$ change, which implies that the variations affect mainly the transverse component (δB_t) (e.g. at barrier 1, $\delta B_t = 50$ nT, while $\delta|B| = 30$ nT).

Fig.1d displays a close-up of $|B|$ for the 4 spacecraft around the main barrier peak marked in Figs.1a–1c by the black box on the horizontal axes. In fact, the barrier is seen almost at the same time by SC1, SC2 and SC3, while SC4 sees it with a clear delay. Moreover, we observe that the barrier is first seen by SC3 starting from 9.486 UT, then by SC1 and later on by SC2. The maximum of the barrier seems to increase from SC3 to SC1, while nothing conclusive in this respect can be said as regards SC2 due to a data gap between 9.4895 to 9.492 UT. A further increase of the barrier peak is observed by SC4 later on during the barrier thinning and rising up to a magnetic field magnitude about twice relative to average level. We set the start of the barrier at SC4 at 9.489 UT and its trailing edge at 9.493 UT. During time lags between SC3, SC1 and SC2, which are smaller than a proton gyroperiod, the barrier shape nearly conserves, while in 2-3 gyroperiods the barrier width and height at SC4 evolve a lot. This proves that the gyroperiod can be taken as the characteristic time scale for estimating (4). Fig.1a further supports this: over similar time intervals barriers 3 and 5 change a lot (the maximun change is for barrier 5 with the maximum lag), while barrier 2 does not change and barrier 4 changes less than barrier 1. Coming back to Fig.1d, the delays between the SC's and their positions allow us to calculate the average speed of the barrier, which results to be $(-32, 40, -36)$ km/s. From the thermal speed of protons and the observed local magnetic field we calculate the proton gyroradius, which, divided by the barrier speed, yields a characteristic barrier time scale of 9 s, depicted under the ρ_i symbol in the figure. We remark that such a time scale roughly agrees with the barrier peak width as seen by SC4 and with the barrier edge scale.

Fig.1e shows the electric field GSE x component, E_x, from SC3 and SC4 for the same time interval as in Fig.1d. E_x displays several narrow peaks, generally associated with large gradients of $|B|$, the most prominent of which are in excess of 4 mV/m and roughly coincide with the trailing edge of the main barrier peak. Similarly to $|B|$, SC4 E_x appears to be shifted in time with a lag of ~ 85 s. Near the main barrier the flow has a complicated 3D pattern: the vortex-like loops in the $V_x - Y_y$ and $V_y - V_z$ planes spread to 80 km/s for an average $|V| \sim 120$ km/s (not shown here).

The E_x and $|\mathbf{B}|$ data at the trailing edge of the barrier main peak allow to perform a check of the rough equality between the cross field velocity and the thermal proton velocity, which is predicted by (4) as a consequence of the finite gyroradius counterbalance of the infinite $|B|$ increase due to the Alfvénic collapse. In fact, the $E/|B|$ ratio yields a value of ~ 260 km/s, which agrees fairly well with the thermal proton velocity near the main barrier $V_{Ti} \sim 220$–290 km/s. This result suggests that actually Alfvénic collapse mitigated by the finite gyroradius effect could account for the observed magnetic barriers. Thus, the detected transverse flows support the equilibrium, in correspondence with (4).

The E_x and $|B|$ variations at the barrier main peak trailing edge allow to calculate the phase velocity of the disturbance as $V_{ph} \propto \delta E/\delta B \sim 110$ km/s, which results to be close to the local Alfvén speed $V_A \sim 150$ km/s. This fact and the transverse character of the disturbances, which we described in the discussion of Fig.1c, justify the name "Alfvénic collapse".

We also notice that similar calculations can be performed for other barriers evidenced so far. For instance, at barrier 2 $V_{ph} \sim 85$ km/sec $\sim V_A$ and at barrier 3 the phase velocity results to be ~ 140 km/s (which is roughly equal to the Alfvén speed in the barrier and twice the Alfvén speed outside the barrier), while at the W_k gradient $V_{ph} > 2V_A$; these small narrow barriers are at the border of the free-flowing plasma and here the E_x step at the border of the moving plasma provides a substantial input to δE_x (cf. [2, 9]).

Fig.1f displays a summary of the observations in the GSE XZ plane. The MP is sketched in its nominal position (solid line indicated by "MPnom", [10]) and in the position where it was first encountered by Cluster at 9.00 UT (dashed line indicated by "MP"). A portion of the outbound orbit is also plotted as a solid line and three times are printed close to it to evidence the SC motion (in this representation the MSH is on the left and the magnetosphere is on the right of the MP). Some prominent velocity vectors are drawn on the orbit or close to it: 1) the Cluster entrance to the proper MSH flow at 9.53 UT (see description of Fig.1b above) is marked by the "MSH" velocity vector, roughly parallel to the nominal MP surface; 2) the next vector to the right is the main barrier velocity (marked by "Barrier"), 3) the A vector represents the plasma velocity measured by the Cluster spacecraft. We notice that the latter two vectors form a large angle which in 3D is $\sim 50°$, which implies that the MSH plasma inside the cusp throat flows at a large angle to the velocity of the magnetic barrier (as it should be for a transparent boundary).

The plasma flows not around a smooth MP, but rather over the indented obstacle (see the shape of the magnetopause marked with "MP" in Fig.1f), that results in the turbulent boundary layer generation (cf. [2]) with an irregular streamlining, for which the Alfvénic collapse should create the high $|B|$ barriers.

Since the small barriers (of type 3) originate in the free flow and drift towards the BL, we suggest that the BL decelerated region with deformed field lines is created by them in a dynamic manner. Small barriers 2–5 also display narrowing and growing, but their growth is limited either by fluctuations in W_k and W_t, or because the ion gyroradius scale is reached at small amplitudes. We infer that for high β strong barriers with dominant W_b (such as barrier 1) would appear sporadically. This scenario agrees with the case of April 2, 1996, when a strong barrier is seen by Interball-1 but is not seen by Magion-4 at about 3000 km distance, while in another case, on April 21, 1996, both satellites observed a strong barrier [2]. In the case of April 2, 1996, a maximum of W_k was observed at the MSH edge of a barrier between flowing and stagnant plasma, close to the magnetopause. Panel (2) of Fig.1 of [2] clearly shows that at such maximum the prediction of equation (4) is fulfilled, as $W_k \sim W_t$ (i.e. $E_{kin} \sim E_{th}$ in the notation of [2]). Thus, we can reinterpret already published and so far unexplained magnetic barriers identified in Interball-1 data in the terms of Alfvénic collapse as the source of the interface barrier.

A more developed barrier pattern is observed by Cluster SC1 on February 2, 2003. Fig.2 shows ram, thermal and magnetic field pressure from 22.6 to 23.45 UT on that day. Contrary to the 24 March 2001 event, here $\beta \leq 1$ apart from the first part when $\beta > 1$. In this case, the 4 SC's are separated by $\sim 1\ R_E$ and move from the Northern cusp towards the MSH through a turbulent boundary layer, as suggested by the high level of fluctuations. On the right hand side of Fig.2 $W_k > W_b > W_t$ (i.e. behind the dusk cusp the MSH flow is super-sonic and super-Alfvénic), while the maximum W_b at the magnetic barriers barely reaches the average values of W_k. On the left hand side of Fig.2 W_k is negligible (which implies a stagnation region) and W_t dominates, while narrow magnetic barriers are superimposed. At 22.8–22.5 UT a structured magnetic barrier is detected, in which the dominant W_b is comparable to W_k in the free-flowing MSH on the right side. In this unique case SC1 slides along the barrier for half an hour, which displays the permanent barrier presence, along with its severe structuring. The characteristic width of the barrier maxima cannot be inferred in this case from a comparison of signals at different SC's, as their distance is close to 1 R_E, so that the correlation between field maxima is < 0.3. However, we tend to believe that

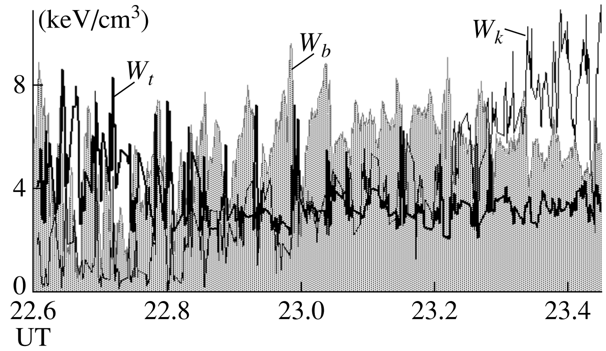

Fig.2. SC1 proton ram pressure (W_k), proton thermal pressure (W_t, thick line), and magnetic pressure (W_b, shadowed line) on February 2, 2003

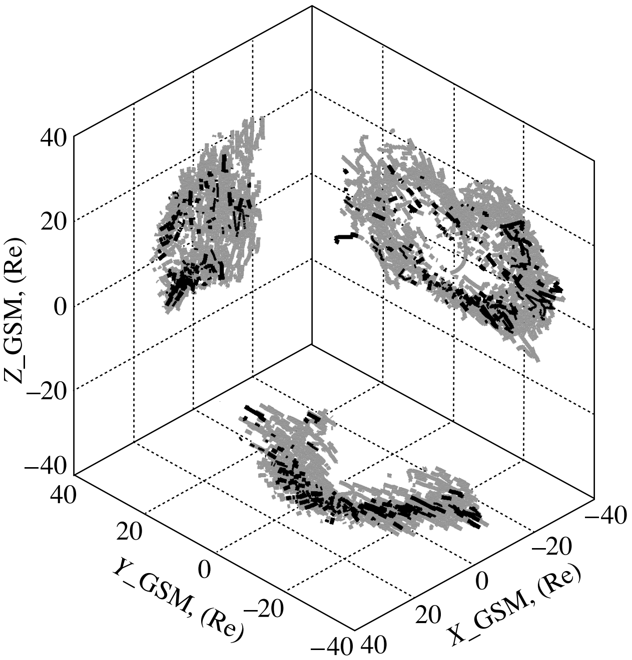

Fig.3. Locations in Geocentric Solar Magnetospheric (GSM) coordinates of 208 magnetic barriers detected in Interball-1 magnetic field data between 1995 and 2000. A correction factor χ was applied in order to account for ram pressure effects (see text for details)

again the width be comparable with the proton gyroradius (cf. Fig.1d). We recall that SC3, being at smaller Z GSE by $1\ R_E$, detected the barrier continuously for less than 10 minutes. Taking this into account along with the Cluster velocity in GSE, one can estimate the barrier width in the MP normal direction as 1000–2000 km. It is well seen that inside the barrier $W_t \sim W_k$, i.e. the plasma flows at about the ion thermal speed, its average angle to the magnetic field is 94°. So, a sonic transverse flow is established in the barrier at equilibrium, in full agreement with the estimate (4). We would like to note, that this very probable Alfvénic collapse occurs over the dusk cusp far from the symmetry GSE X axis, which is similar to what is observed in numerical experiments [6] for the 3D velocity diverging. In our case in the stagnant flow (left side of Fig.2) $\beta > 1$ (cf. [4]), while in the free flow and in the barrier it is not so. In this respect, we refer to [11], who predict an Alfvénic wave structuring for the β detected there with similar magnetic barrier growing. Thus we suggest that Alfvénic collapse is a rather common phenomenon at any β, but this has to be verified through a comprehensive computer modeling. In spite of the lack, until now, of a self-consistent theoretical approach, the experimental data reproduces a number of substantial predicted features, pointing to the necessity of further theoretical and computational efforts. At the MHD scale of the barrier width ($\sim$ 1500 km $\sim$ 10 ρ_i) the frozen-in conditions should be satisfied, that gives average transverse electric fields of 7.4 mV/m in the MP frame for the measured average cross-field drift. For the turbulence seen, part of the ions with gyroradius comparable with the fluctuation characteristic scale, should be subjected to effective collisions with the waves [10], that result in an energy gain of 10–30 keV by the ions, shifting in the electric field direction across the BL. The latter accounts for the enhanced energetic ion fluxes in the turbulent boundary layer [12]. The Alfvénic collapse produces a low β region inside the main barrier (see Fig.1d), that can result in appearance of the accelerated parallel plasma jets due to plasma extrusion by the rising magnetic field [9, 10].

4. Concluding the Letter, in Fig.3 we present the statistical barrier distribution in 3 planes in the Geocentric Solar Magnetospheric frame of reference from MSH Interball-1 data for the 1995–2000 period. The locations have been corrected taking into account the solar wind ram pressure $P_{\rm ram}$: the spacecraft coordinates, X_{GSM}, Y_{GSM} and Z_{GSM}, are multiplied by $\chi = P_{ram}^{1/6}$; however, the correction is applied only to Y_{GSM} and Z_{GSM} when $X_{GSM} < 0$. Grey shadowing illustrates the orbit coverage: orbit traces in the MSH with magnetic disturbances power being in $\sim$ 1.5 over the average fluctuations in the background flow. Thin black lines show the detection of barriers with amplitude 20–50 nT over the average $|B|$, while thick lines show the detection of barriers with amplitude exceeding the average $|B|$ by more than 50 nT. We have excluded bow shock crossings and those magnetopause back-and-forth crossings, in which the magnetic maximum exceeded the magnetic field just inside the magnetosphere by less than 30 per cent; also the barriers with duration over 10 minutes have been discarded from the data set with 1–4 Hz sampling. One can see, that on the dayside the barriers tend to occur at higher latitudes where the flux velocity rises and the flow interacts with 3D cusp throat. The barriers tend to be more frequent at the dawn magnetospheric flanks (with negative Y). Near the equator there is another group of barriers in the geomagnetic tail at $X < -10R_E$, where the neutral sheet with a weak magnetic field starts to perturb the 2D MSH flow in three dimensions. Thus, strong barriers with magnetic field enhancement over the average field strength at the high latitudes or in the tail MSH, represent a regular feature of streamlining of the plasma flow around the deformed boundaries with 3D feature.

In conclusion, we acknowledge that the theoretical description of Alfvénic collapse is to be improved for smaller plasma β and stronger gradients, but wish to remark that intercomparison of theory, modelling and experimental data points out that Alfvénic collapse is in general a promising mechanism for magnetic field generation. The magnetic field line pile-up (breaking) is predicted to operate also in astrophysical and heliospheric plasma flows with the divergent transverse velocity, e.g. this mechanism can account for magnetic field filamentation and rise at the convection cell boundaries on the Sun [3].

5. We are grateful to P.L. Sulem and T. Passot for useful discussions. This work was partially supported by ISSI (Team 81), INTAS # 03-50-4872, INTAS # 05-1000008-8050, RFBR # 06-02-17256, RFBR # 06-01-00665, KBN # 8T12 E 016 28, and ECRT Network HPRN-CT-2001-0314.

1. G. Haerendel, J. Atmos. Terr. Phys. **40**, 343 (1978).
2. S. P. Savin, L. M. Zelenyi, S. A. Romanov et al., Pis'ma v ZhETF, **74**, 547 (2001).
3. A. Title, In: *AIP Conf. Proc.* **703**: *Plasmas in the Laboratory and in the Universe: New Insights and New Challenges*, Eds. G. Bertin, D. Farina, and R. Pozzoli, 2004, p. 163.
4. E. A. Kuznetsov, T. Passot, and P. L. Sulem, Phys. Plasmas **11**, 1410 (2004).
5. E. A. Kuznetsov and V. P. Ruban, ZhETF **91**, 775 (2000) [JETP **91**, 775 (2000)].
6. V. A. Zheligovsky, E. A. Kuznetsov, and O. M. Podvigina, Pis'ma v ZhEFF **74**, 367 (2001) [JETP Letters **74**, 367 (2001)].
7. E. A. Kuznetsov, J. Nonlin. Math. Phys. **13**, 64 (2006).
8. C. P. Escoubet, C. T. Russel, and R. Schmidt, Sp. Sci. Rev. **79**, 1 (1997).
9. S. P. Savin, L. M. Zelenyi, E. Amata et al., Pisma v ZhETF **79**, 452 (2004).
10. S. Savin, E. Amata, M. Andre et al., Nonlin. Processes Geophys. **11**, 377 (2006).
11. G. Bugnon, R. Goswami, T. Passot, and P. L. Sulem, Adv. Space Res. **38**, 93 (2006).
12. T. Asikainen and K. Mursula, Ann. Geophysicae **23**, 2217 (2005).